Available online at www.sciencedirect.com

SciVerse ScienceDirect

Ceramics International 39 (2013) 143–151

CERAMICS INTERNATIONAL

www.elsevier.com/locate/ceramint

Low temperature processed SnO_2 films using aqueous precursor solutions

Na Cai, Junghyun Cho*

Department of Mechanical Engineering and Materials Science and Engineering Program, State University of New York (SUNY) at Binghamton, Binghamton, NY 13902-6000, United States

Received 29 May 2012; accepted 1 June 2012
Available online 13 June 2012

Abstract

We present a comparison study of the microstructure developments during aqueous solution deposition of SnO_2, particularly, through chemical bath deposition (CBD) and liquid phase deposition (LPD) at very low temperatures (40–75 °C). The effects of solution chemistry on the microstructural details and electrical properties of SnO_2 thin films are presented and discussed. Smooth, nanoparticulate SnO_2 films were obtained from supersaturated precursor solutions with lower precursor concentrations while more aggregated SnO_2 films were generated from higher precursor concentrations. Loosely-packed and porous structures were obtained from low supersaturation solutions with very low pHs. The deposition rates were also evaluated under various deposition conditions. XRD result shows that annealing process helps improve the degree of crystallinity of the as-deposited films that are composed of 3–10 nm nanocrystalline particles. One advantage of LPD of SnO_2 films is *in-situ* fluorine doping during deposition. The resulting electrical resistivity of F-doped SnO_2 films was about 18.7 Ω cm after the films were annealed at 450 °C.

Keywords: CBD; LPD; Aqueous solution; SnO_2

1. Introduction

Nanostructured semiconducting oxides have attracted considerable interests due to its unique properties and applications. Among such semiconductors, tin oxide (SnO_2) is one of the promising candidates for many applications due to its outstanding chemical, optical and mechanical properties. SnO_2 behaves like an n-type semiconductor with various microstructure and morphology, which can be applied to such applications as gas sensors [1–3]. By tailoring various nanostructures of SnO_2 thin film, the sensitivity and selectivity towards specific gas are improved. SnO_2 is also a good candidate for UV luminescent material [4,5] due to its wider band gap ($E_g = 3.67$ eV) and smaller exciton Bohr radius ($a_B = 1.7$ nm). SnO_2 by coating with a thin layer of ZnO, TiO_2 or other semiconducting oxides can be used for solar cell applications, exhibiting good energy conversion efficiencies and long-term stability [6–8]. Mesoporous SnO_2 spheres with tunable particle size has also shown a good potential to achieve high photoconversion efficiency [9]. Therefore, having the capability to tailor microstructures and surface morphologies is essential in the above applications in order to meet the performance requirements.

Size- and shape-controlled antimony-doped tin oxide nanoparticles has also shown some advantages over TiO_2 based electrochromic devices due to its improvement in a fast-switching response which is one of the crucial aspects for commercial applications of this device [10–12]. In addition, field effect transistors (FETs) provide another opportunity for SnO_2 materials [13–15]. Through the conventional lithography and lift-off processes, low-cost metal-oxide-semiconductor FETs can be fabricated. This technology is not only useful for the development of on-screen electronic devices, but also gives great interesting opportunities for the FET-like gas sensors [16]. One of the important properties of SnO_2 is its transparency while exhibiting conductivity with the proper doping to form a transparent conducting oxide (TCO) film such as fluorine doped tin oxide (FTO) [17–19] and antimony doped tin oxide (ATO) [20–22].

*Corresponding author.
E-mail address: jcho@binghamton.edu (J. Cho).

0272-8842/$36.00
http://dx.doi.org/10.1016/j.ceramint.2012.06.002

Various techniques have been developed to fabricate tin oxide thin films including spray pyrolysis [23,24], magnetron sputtering [25,26], chemical vapor deposition [27] and sol–gel coating [21,28,29]. All these techniques listed involve high temperature processing or post-annealing conditions. As a result, the choice of substrates is limited. The coating techniques being capable of depositing high-quality ceramic films at low temperatures are therefore needed as more flexibility for choosing substrates including temperature sensitive materials will be of considerable interest these days. Given that, chemical bath deposition (CBD) [30–33] and liquid phase deposition (LPD) [34–36] provide a sensible alternative to conventional processes since both of them can achieve high controllability of film thickness and morphology and have low temperature processing capability with simple and low cost instrumentation, have low energy consumption and use less hazardous chemicals.

In our study, a capability to tailor nano- and microstructures in such low-temperature solution processes was developed by means of solution chemistry that controls nucleation and growth of nanoparticles. CBD was utilized to fabricate undoped SnO_2 films while an LPD technique was employed to fabricate *in-situ* fluorine-doping in tin oxide films, which eliminates an additional process for doping. These tin oxide films were successfully deposited on both glass and plastic substrates. Various surface morphologies and properties obtained from different solution conditions are discussed in the following sections.

2. Experimental methods

2.1. Treatment of the substrate

The substrates used in this study were 0.2 mm thick microscope cover glass (VWR International), and polyethylene terephthalate (PET). The glass slides or PET were cut into ca. 11 mm × 11 mm samples. The substrates were ultrasonicated in acetone for 20 min, then rinsed by DI water and dried completely with nitrogen gas, followed by cleaning in oxygen plasma for 20 min. The plasma treatment also made the substrate surface hydrophilic.

2.2. Chemical bath deposition of SnO_2 films

The deposition of SnO_2 films was carried out at near-room temperature. Tin tetrachloride ($SnCl_4$, 99.99%, Alfa Aesar, Ward Hill, MA) and hydrochloric acid (HCl, 36.5–38%, J.T. Baker, Phillipsburg, NJ) were used as received without further purification. Appropriate amount of concentrated HCl was first added to ice-cold deionized (DI) water and then tin tetrachloride was added to the HCl solution while stirring was applied. Finally, additional cold DI water was added and the as-prepared solutions were stored in refrigerator (4 °C) before use. The detailed precursor solution conditions are given in Table 1.

The glass substrates were placed vertically in a polytetrafluoroethylene (PTFE) sample holder which was immersed in the $SnCl_4$ precursor solution. The deposition apparatus was kept in a constant temperature oil bath set at 75 °C. A stepwise deposition process was implemented by changing the precursor solution with a freshly prepared one every 1 h. No forced stirring was applied to the solutions during deposition. After the desired steps, the substrates were taken out from the sample holder and rinsed and ultrasonicated with anhydrous ethanol for 1 min, followed by complete drying with nitrogen gas.

2.3. Liquid phase deposition of SnO_2 films

The precursor solution was prepared by dissolving a certain amount of tin(II) fluoride (SnF_2) in hydrofluoric acid (HF) aqueous solution. Then hydrogen peroxide (H_2O_2) aqueous solution was added to the mixture. H_2O_2 used in this study acts as the oxidant reagent of tin ionic dissolving species for stabilized Sn(IV)–fluorine complex. Boric acid (H_3BO_3), dissolved in DI water, was used as an initiator (F^- scavenger). The precursor and its initiator were mixed together with stirring just before the experiment started. The glass or PET substrates were placed vertically in the sample holder. The deposition setup and processes were the same as those of CBD.

2.4. Characterizations of thin films

The microstructure and morphology of the as-deposited SnO_2 films were characterized by using field emission SEM (Supra 55 VP, Carl Zeiss). Impurity content was examined by energy dispersive X-ray spectrometry (EDS; EDAX Inc., Mahwah, NJ) analysis with FE-SEM. Cross-sectional SEM specimens were prepared by fracturing the brittle glass substrates with the film. The crystallinity of the films was characterized by an X-ray diffractomer (XRD; Scintag

Table 1
Precursor solution conditions, as-deposited film thicknesses and annealing conditions with two processing techniques.

Processing technique	Substrate	Precursor solution condition	Film thickness (nm)	Heat treatment condition
CBD	Glass, Silicon	$[SnCl_4]$ = 1.0–15.0 mM; $[HCl]$ = 10.0–199.0 mM; T = 75 °C	40–308	Up to 450 °C, 2 h for each temperature, heating rate 10 °C/min
LPD	Glass, PET*	$[SnF_2]$ = 5–60 mM; $[HF]$ = 20–240 mM; $[H_2O_2]$ = 5–60 mM; $[H_3BO_3]$ = 30–230 mM; T = 40–60 °C	100–315	Up to 450 °C, 2 h for each temperature, heating rate 10 °C/min

*Due to glass transition temperature, SnO_2 film grown on PET was annealed at 100 °C.

XDS 2000) with Cu Kα radiation with wavelength $\lambda = 1.541$ Å. The diffraction angle 2θ was varied from 10 ° to 90 ° by step of 0.02 ° and scanning rate was fixed at 0.3 °min^{-1}. The electrical resistivity was measured using the standard van der Pauw four probe method. Colloidal silver paste was used for the top electrodes.

3. Results and discussion

3.1. Chemical bath deposition (CBD)

3.1.1. Effect of preparation conditions on the morphology of as-deposited film

Generally, the hydrolysis of Sn^{4+} ions in the solution is described with the following reaction:

$$Sn^{4+} + 2H_2O \rightleftarrows SnO_2 + 4H^+ \quad (1)$$

From the reaction, Sn^{4+} concentration ($[Sn^{4+}]$), pH and temperature are the three key parameters to control the film formation and microstructure. Since temperature was fixed at 75 °C in our CBD process, we would discuss the $[Sn^{4+}]$ and pH effects separately. Fig. 1(a) and (b) shows representative SnO_2 morphologies prepared at different $[Sn^{4+}]$'s with a fixed HCl concentration. Particle attachment through bulk precipitation seemed to be the controlling mechanism for film formation. The best surface morphology with smooth and fine particulate surface formed with the solution condition of 2.0 mM $SnCl_4$ and 10.0 mM HCl (Fig. 1(a)). With the higher $[Sn^{4+}]$, a higher degree of supersaturation of the precursor solution reaches, which promotes more homogenous nucleation of SnO_2. Therefore, aggregation occurs frequently among those growing particles which causes the film surface to display a rougher morphology (Fig. 1(b)). Compared to particle sizes ranging from 5 to 10 nm in Fig. 1(a), the average particle size at higher $[Sn^{4+}]$ is larger between 10 and 20 nm.

Fig. 1(a) and (c) indicates the pH effect on microstructure and morphology of as-deposited films. From reaction (1), it can also be expected that the chemical equilibrium is retarded toward the right side by increasing the concentration of HCl. Hence, increasing HCl concentration yields fewer nuclei and a slower precipitation rate which leads to mild particle growth in the solution without being aggregated with others. Further, they get more opportunity to be attached to the substrate under low pH. At high pH (i.e., at low HCl concentration), however, the particle cluster gets larger, and if it is larger than a certain size, it would not be attracted to the substrate. Fig. 1(c) shows a loose-packed porous film, in which the particle size is about 20–30 nm. The precursor solution in this case has a larger [HCl] with a lower pH = 0.66. The value of pH was measured right after the precursor solution was prepared.

Therefore, the microstructure and surface morphology of the as-deposited SnO_2 films are significantly affected by the precursor solution conditions. More bulk precipitation occurs in high $[Sn^{4+}]$ that can make the surface quite rough as shown in Fig. 1(b). At very low supersaturation by adding more HCl (as is the case for Fig. 1(c)), we have also observed bigger aggregated particles that lead to increased roughness. This indicates that while extensive bulk precipitation can be avoided at low supersaturation obtained from very low pH solution, relatively small particles available in the solution can grow and then be attracted to the growing film surface quite strongly and randomly. Importantly actual attachment of those formed particles in solution will also be dependent on the colloidal forces such as DLVO force [37,38] and therefore solution pH should play an important role in arranging the particles on the growing films since their surface charges are dependent on the pH of the precursor solution. The iso-electric point (IEP) of SnO_2 can be about 5.5–6.0 [39],

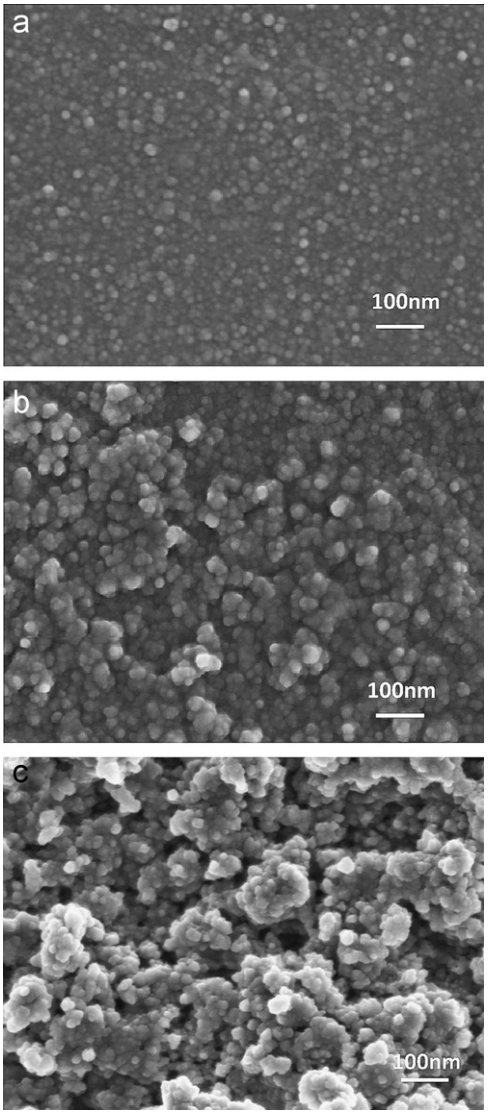

Fig. 1. SEM images of the as-deposited SnO_2 films under various precursor solution conditions at 75 °C: (a) 2.0 mM $SnCl_4$ + 10.0 mM HCl solution; (b) 15.0 mM $SnCl_4$ + 10.0 mM HCl solution; (c) 2.0 mM $SnCl_4$ + 199.0 mM HCl solution.

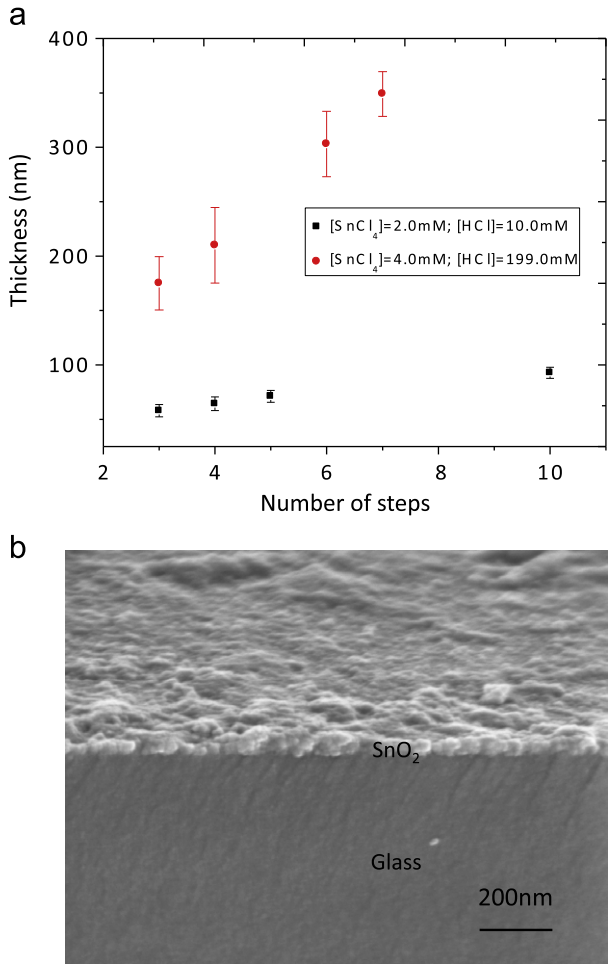

Fig. 2. (a) Film thickness as a function of deposition steps. Precursor solution condition is $[SnCl_4]=2.0$ mM, $[HCl]=10.0$ mM; and $[SnCl_4]=4.0$ mM, $[HCl]=199.0$ mM. (b) One example of cross-sectional SEM image of the as-deposited SnO_2 films.

so it is expected that very low pH will result in highly positively charged SnO_2 particles in solution.

3.1.2. Structural analysis of SnO_2 films

Fig. 2(a) shows film thickness as a function of deposition steps. Each step lasted for 1 h since the film did not grow much after deposition of 1 h. This is because the particles formed by homogeneous nucleation in the precursor solution are attracted to the properly treated substrate surface as a result of colloidal interactions before they grow into larger colloidal particles. In fact, after 1 h processing, the small particles which can be attracted are depleted and the film growth rate almost saturates. Film thickness increases linearly with the number of steps when the solution is changed with the freshly prepared one. With a linear fitting, the deposition rate was calculated from 5 nm/step (for mid-level supersaturation) to 44 nm/step (for low supersaturation). The latter case was achieved with the addition of large HCl concentration to the solution. Fig. 2(b) shows one example of the cross-sectional SEM view of a CBD SnO_2 film whose thickness is around 70 nm.

The XRD patterns of the as-deposited (75 °C) and annealed SnO_2 film (450 °C) are presented in Fig. 3. The broad peaks indicate amorphous or nanocrystalline nature of the film at the deposition temperature. Cross-sectional high-resolution TEM image of the as-deposited SnO_2 films (not shown here) indeed demonstrates that the film contains densely-packed SnO_2 nanocrystallites of ~5 nm size. After as-deposited films were annealed at 450 °C for 2 h in air, crystallinity of the films improved as the peaks were getting sharper and more distinct from the background. The average crystal size, as estimated by the Scherrer equation, is in the range 6–10 nm after 450 °C annealing. EDS analysis confirmed the absence of residual Cl in the films within its detectability limit.

3.2. Liquid phase deposition

3.2.1. Effect of the precursor solution on the morphology of as-deposited film

Liquid phase deposition refers to the formation of oxide thin film from an aqueous solution of a metal–fluoro complex $[MF_n]^{m-n}$ which is slowly hydrolyzed by adding water, boric acid (H_3BO_3) or aluminum metal. While the addition of water directly forces precipitation of the oxide, boric acid acts as a fluorine scavenger, which destabilizes the fluoro complex and forces the oxide precipitation. In particular, tin–fluoro complex can involve the following equilibrium reactions [40]:

$$SnF_2+4HF+H_2O_2\rightarrow[SnF_6]^{2-}+2H_3^+O \quad (2)$$

$$[SnF_6]^{2-}+nH_2O\rightleftarrows[SnF_{6-n}(OH)_n]^{2-}+nHF \quad (3)$$

$$[SnF_{6-n}(OH)_n]^{2-}+(6-n)H_2O\rightleftarrows[Sn(OH)_6]^{2-}+(6-n)HF \quad (4)$$

$$[Sn(OH)_6]^{2-}+2H^+\rightarrow SnO_2+4H_2O \quad (5)$$

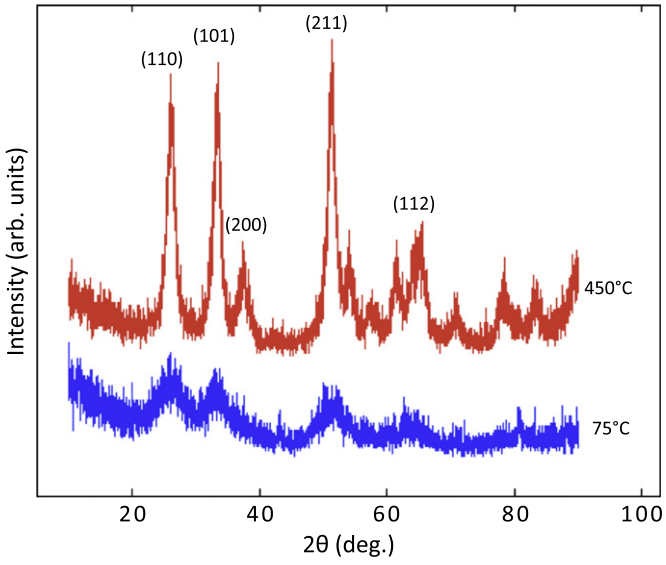

Fig. 3. XRD patterns of as-deposited (at 75 °C) and annealed (at 450 °C) SnO_2 films.

$$H_3BO_3 + 4HF \rightarrow BF_4^- + H_3O^+ + 2H_2O \quad (6)$$

Fig. 4(a) and (b) shows the film morphologies with two different tin–fluoro complex concentrations. We achieved higher $[SnF_6]^{2-}$ by adding more SnF_2 powder, HF, and H_2O_2 solution while keeping $[Sn^{2+}]/[F^-]$ ratio to 1/6 and $[Sn^{2+}]/[H_2O_2]$ ratio to 1/1. With lower $[SnF_6]^{2-}$, the SnO_2 film shows denser underlying structure that contains finer particles (< 25 nm) but larger adsorbed particles (~40 nm) and less aggregated clusters. With higher $[SnF_6]^{2-}$, on the other hand, the SnO_2 film exhibits more porous structure with relatively larger particles (~60 nm) and more aggregated clusters. It can be expected that the hydrolysis of $[SnF_6]^{2-}$ shifts the reaction toward the right by increasing its concentration, which leads to more bulk precipitates through homogeneous nucleation in solution, thereby resulting in more aggregation on the films. Higher $[SnF_6]^{2-}$ can provide a larger driving force for nucleation because of a higher degree of supersaturation.

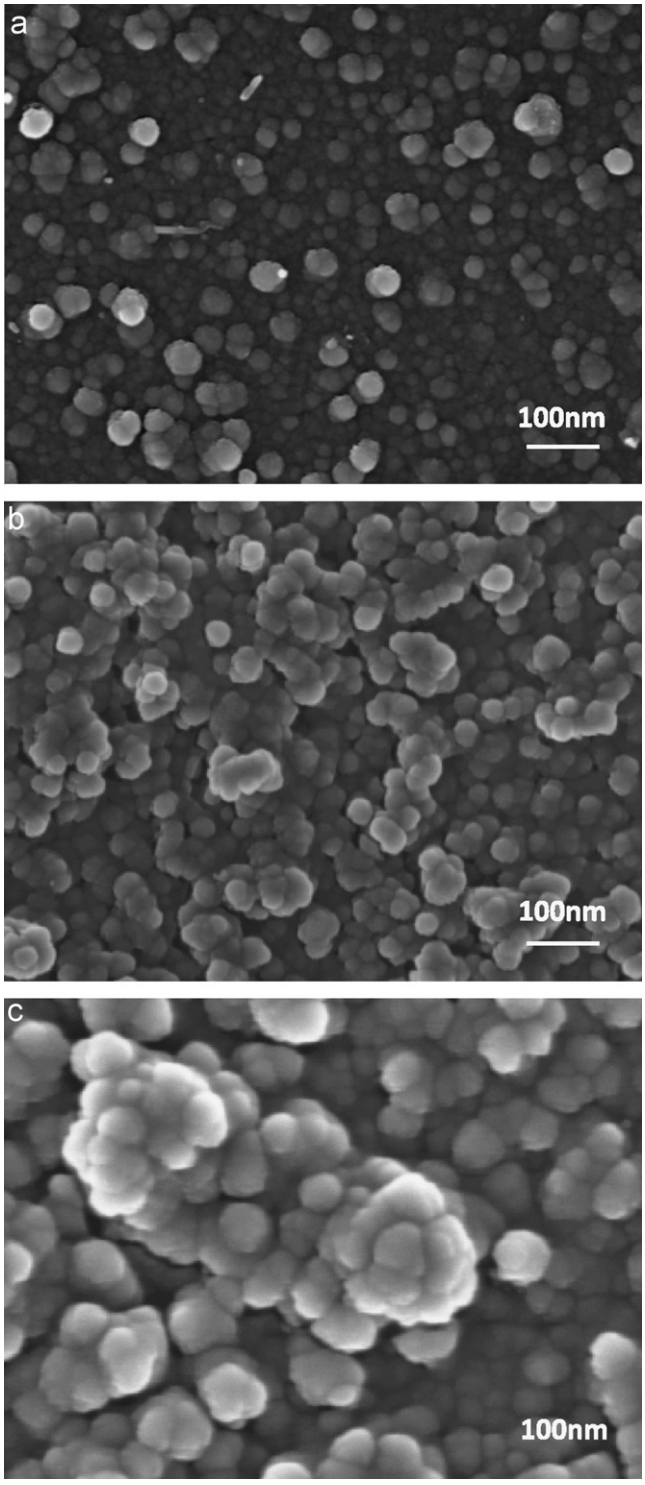

Fig. 4. SEM images of the as-deposited SnO_2 films at fixed $[F^-]/[Sn^{2+}]$ = 6/1 at 60 °C: (a) $[SnF_2]$ = 5 mM, $[H_3BO_3]$ = 30 mM; (b) $[SnF_2]$ = 10 mM, $[H_3BO_3]$ = 30 mM; (c) $[SnF_2]$ = 10 mM; $[H_3BO_3]$ = 230 mM.

Boric acid is an F^- scavenger which shifts the equilibrium reactions to the right hand side. Hence, the amount of H_3BO_3 should be one of the key factors in the LPD process. As expected, larger particles and strong aggregation appeared to occur on the film surface with higher $[H_3BO_3]$ because of a large driving force for the nucleation and growth of SnO_2 particles in such solution conditions, as shown in Fig. 4(b) and (c). High supersaturation was therefore achieved by adding more boric acid that depletes HF in the solution. Its morphology shows a more porous and loosely-packed microstructure.

Compared to CBD, current precursor solution condition for LPD seemed to involve a higher degree of supersaturation as the solution became more turbid in the same duration of deposition. The films become more particulate and thus rougher with the degree of supersaturation. Adding more SnF_2 or H_3BO_3 in the LPD process in fact yielded the same effect as in the CBD case with higher $[Sn^{4+}]$ by adding more $SnCl_4$. Fig. 5 depicts a deposition mechanism that can possibly explain nanoparticle-based film morphologies grown from the supersaturated solution. Actual particle attachment and surface morphologies, however, also seemed to be controlled by nanoparticle–substrate (or growing film once the substrate is covered with SnO_2)

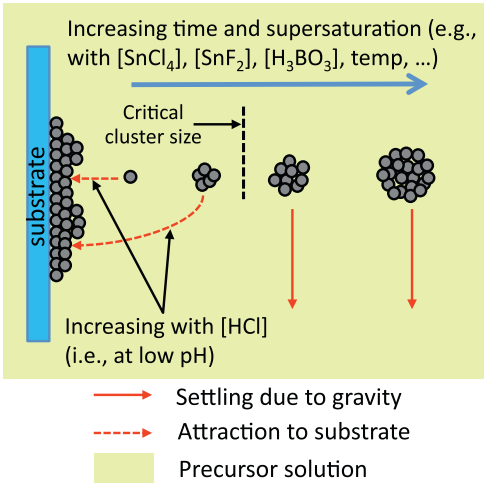

Fig. 5. Schematic of the deposition mechanism that involves nucleation, growth, and aggregation. Critical cluster size defines the particle size small enough to be attracted to the substrate.

interactions that can increase or decrease depending on their surface charges, which are very sensitive to pH of the precursor solution.

As we mentioned before, one of the advantages of aqueous solution deposition is low-temperature process. As a result, PET substrate whose glass transition temperature is ~70 °C [41] can be utilized without any possibility for its degradation during deposition. Fig. 6 shows the surface morphologies of the films grown on PET and glass substrates. When the precursor condition was the same, similar nanoparticulate structure was observed for the film on PET substrate, compared to that on the glass substrate. It proves the potential of current processing protocol to be used for flexible substrates, as well as for rigid substrates.

3.2.2. Structural analysis of SnO_2 thin films

The film growth rate under a specific LPD solution condition is shown in Fig. 7. Compared to the precursor solution condition discussed in Section 3.2.1, this LPD solution has a higher degree of supersaturation. Step-wise approach was employed with 1 h per step in order to avoid

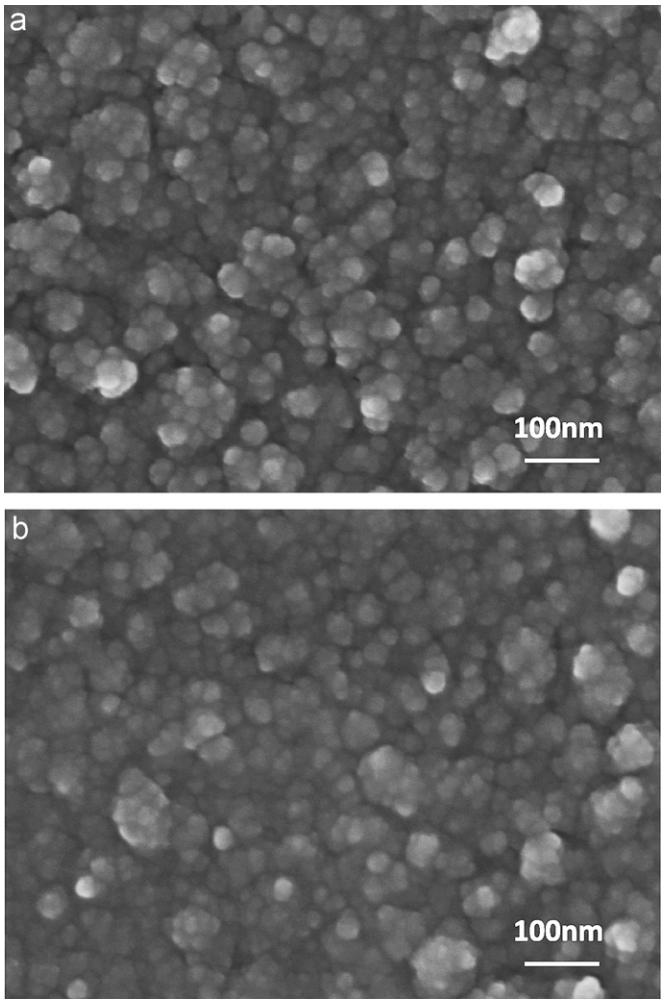

Fig. 6. SEM images of the as-deposited SnO_2 films prepared from $[SnF_2]=60$ mM, $[F^-]/[Sn^{2+}]=6/1$, and $[H_3BO_3]=230$ mM at 40 °C on two different substrates: (a) PET; (b) glass.

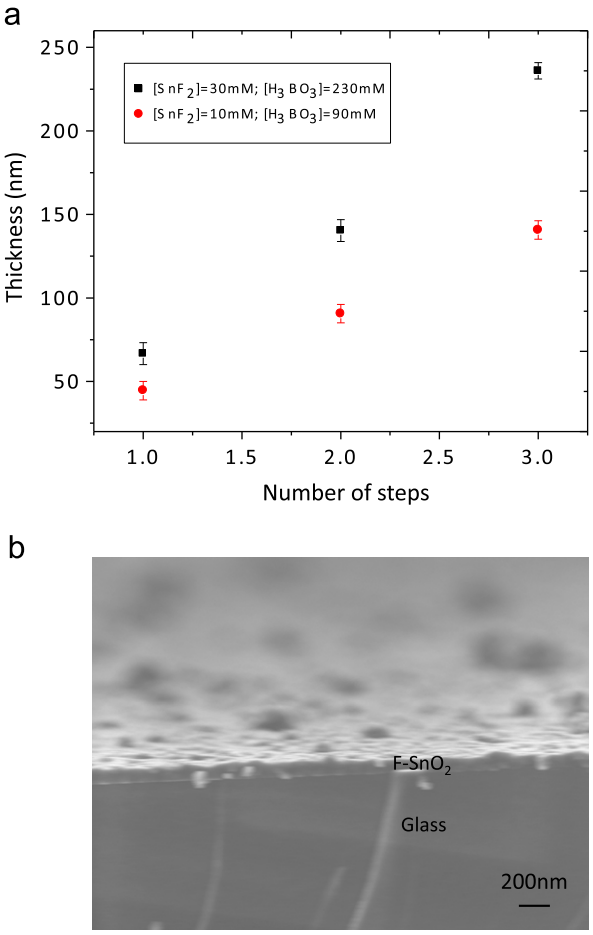

Fig. 7. (a) Film thickness as a function of deposition steps. Precursor solution condition was $[SnF_2]=30$ mM, $[Sn^{2+}]/[F^-]=1/6$, $[H_3BO_3]=230$ mM and $[SnF_2]=10$ mM, $[Sn^{2+}]/[F^-]=1/6$, $[H_3BO_3]=90$ mM. (b) One example of cross-sectional SEM image of the as-deposited $F-SnO_2$ films.

the depletion of the particles which are small enough to be attracted to the surface of the film. The deposition rate seemed to be accelerated, and were from 48 to 87 nm/step on average based on the varying solution conditions. Higher deposition rate reaches by the addition of SnF_2 and H_3BO_3. Fig. 7(b) shows one example of the cross-sectional SEM view of an LPD SnO_2 film whose thickness is around 110 nm. Here, a few large aggregated clusters are shown on the film surface, which can be excluded via more stringent solution control to yield a smoother film.

The crystal structure of the SnO_2 thin films fabricated by LPD was also investigated. The XRD patterns of the as-deposited (40 °C) and annealed SnO_2 films are presented in Fig. 8. As-deposited films were annealed at a temperature of 100 °C, 250 °C or 450 °C for 2 h in air. Due to its quite low solution temperature, the as-deposited film displays more amorphous nature, compared to the as-deposited films prepared by CBD at 75 °C. The peaks shown on the annealed samples are getting sharper and more visible from the background. It indicates that the crystallinity of the films improves with the annealing temperature. The average crystal size, as estimated by the Scherrer equation, is in the range of 3–5 nm after 250 °C while 6–10 nm after

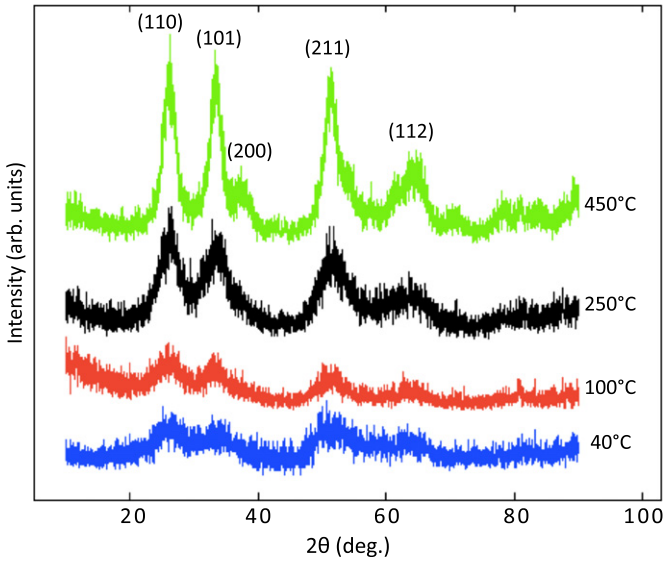

Fig. 8. XRD patterns of as-deposited (at 40 °C) and annealed SnO_2 films (at 100 °C, 250 °C, and 450 °C).

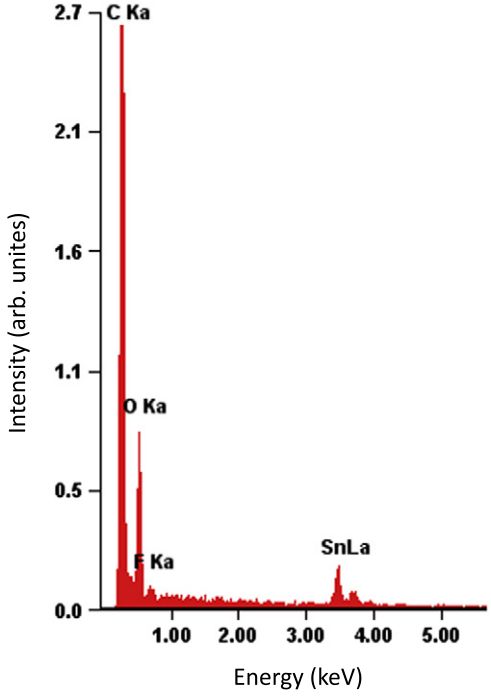

Fig. 9. EDS analysis of LPD SnO_2 film.

450 °C annealing. The sample after annealing at 100 °C did not significantly increase its crystallinity. In addition, an EDS spectrum confirmed the presence of fluorine in the film as shown in Fig. 9.

3.3. Electrical property of low-temperature processed SnO_2 films

In order to produce SnO_2 thin films for electronic applications, electrical conductivity is one of the crucial parameters. While as-deposited films were annealed at up to 450 °C for 2 h in air, the longer annealing treatment times did not further reduce the electrical resistivity. The resistivity of as-deposited and heat-treated films with two processing techniques is shown in Table 2. The resistivity of the as-deposited thin film by CBD processing was too high to be measured. The resistivity of the annealed film was 2.93×10^3 Ω cm. On the other hand, LPD SnO_2 film shows a higher electrical conductivity due to the fluorine doping. After heat treatment, it decreased to 18.7 Ω cm. Compared to other literature electrical conductivity values [42,43], our low-temperature processed films have relatively high resistivity. This is probably due to the difficulty in forming high crystalline films and the strong interaction between the carriers and the interfaces and defects resulting from nanoparticles. The grain size reported in Agashe's work [43] is ~230 nm which is much larger than the current study. Another possibility which can further improve the film conductivity is the film thickness. We have so far grown the LPD SnO_2 film with a thickness up to 250 nm without film cracks. Therefore, in order to have more conductive films from low-temperature solution processing, the next step should be directed at depositing a thicker, denser, and crack-free SnO_2 film, along with larger grain structures.

4. Conclusions

Nanostructured SnO_2 thin films were deposited on glass substrates from two aqueous solution deposition techniques at very low temperatures (40–75 °C). Solution chemistry provides a good insight to understand the morphology of the resulting thin films. In particular, supersaturation and pH play an important role in controlling the morphology of the thin films. Interactions among the particles and the growing films need to be better understood to obtain more quantitative microstructure predictions. The as-deposited SnO_2 films

Table 2
Comparison of electrical resistivity of as-deposited and annealed films with two deposition procedures.

Processing technique	Solution condition	Film thickness (nm)	Electrical conductivity	
			As-deposited	Heat treated (at 450 °C)
CBD	$[SnCl_4]=2$ mM; pH = 2.0; $T=75$ °C	93	Not measurable	2.93×10^3 Ω cm
LPD	$[SnF_2]=5$ mM; $[Sn^{2+}]/[F^-]=1/6$; $[H_3BO_3]=15$ mM; $T=60$ °C	254	4.0×10^4 Ω cm	18.7 Ω cm

consist of crystalline SnO_2 nanoparticles. After heat treatment, the crystal size increases. Specifically, LPD processing gives a deposition method which can *in-situ* dope F^- to SnO_2 thin films with the resistivity of $\sim 18.7\,\Omega\,cm$. EDS results confirmed the presence of small amount of fluorine in the film. In addition, thin SnO_2 films were fabricated on a PET substrate with the similar microstructure and morphology using the same low temperature processing.

Acknowledgments

This work was partially supported by the Center for Advanced Microelectronics Manufacturing (CAMM). SEM work was carried out in Analytical and Diagnostics Laboratory (ADL) at SUNY, Binghamton.

References

[1] J.H. Jeun, S.H. Hong, CuO-loaded nano-porous SnO_2 films fabricated by anodic oxidation and RIE process and their gas sensing properties, Sensors and Actuators B 151 (2010) 1–7.
[2] M. Yang, S.H. Hong, Fabrication of ITO/SnO_2 two-layer thin films and their gas sensing properties, Journal of the Electrochemical Society 157 (2010) J392–J396.
[3] L. Liu, C.C. Guo, S.C. Li, L.Y. Wang, Q.Y. Dong, W. Li, Improved H_2 sensing properties of Co-doped SnO_2 nanofibers, Sensors and Actuators B 150 (2010) 806–810.
[4] T. Hayakawa, T. Enomoto, M. Nogami, Nanocrystalline SnO_2 particles and two fold-coordinated Sn defect centers in sol–gel-derived SnO_2-SiO_2 glasses, Journal of Materials Research 17 (2002) 1305–1311.
[5] B.L. Yu, C.S. Zhu, F.X. Gan, Exciton spectra of SnO_2 nanocrystals with surficial dipole layer, Optical Materials 7 (1997) 15–20.
[6] A. Kay, M. Gratzel, Dye-sensitized core–shell nanocrystals: improved efficiency of mesoporous tin oxide electrodes coated with a thin layer of an insulating oxide, Chemistry of Materials 14 (2002) 2930–2935.
[7] K. Tennakone, G.L.M.P. Apsonsu, Y.P.Y.P. Ariyasinghe, R.C. Buchanan, V.P.S. Perera, H. Tennakone, T.R.C.K. Wijayarathna, Dye-sensitized solar cells based on nanostructured semiconductor oxide ceramics with ultra-thin barrier layers, Integrated Ferroelectrics 115 (2010) 120–131.
[8] W.P. Tai, K. Inoue, J.H. Oh, Ruthenium dye-sensitized SnO_2/TiO_2 coupled solar cells, Solar Energy Materials and Solar Cells 71 (2002) 553–557.
[9] A. Hossain, G.W. Yang, M. Parameswaran, J.R. Jennings, Q. Wang, Mesoporous SnO_2 spheres synthesized by electrochemical anodization and their application in CdSe-sensitized solar cells, Journal of Physical Chemistry C 114 (2010) 21878–21884.
[10] H.J. Kim, J.K. Seo, Y.J. Kim, H.K. Jeong, G. Il Lim, Y.S. Choi, W.I. Lee, Formation of ultrafast-switching viologen-anchored TiO_2 electrochromic device by introducing Sb-doped SnO_2 nanoparticles, Solar Energy Materials and Solar Cells 93 (2009) 2108–2112.
[11] M. Pflughoefft, H. Weller, Spectroelectrochemical analysis of the electrochromism of antimony-doped nanoparticulate tin-dioxide electrodes, Journal of Physical Chemistry B 106 (2002) 10530–10534.
[12] B. Orel, U.L. Stangar, U. Opara, M. Gaberscek, K. Kalcher, Preparation and characterization of Mo-doped and Sb-Mo-doped SnO_2 sol–gel-derived films for counterelectrode applications in electrochromic devices, Journal of Materials Chemistry 5 (1995) 617–624.
[13] T.H. Cui, F. Hua, Y. Lvov, FET fabricated by layer-by-layer nanoassembly, IEEE Transactions on Electron Devices 51 (2004) 503–506.
[14] U. Lampe, E. Simon, R. Pohle, M. Fleischer, H. Meixner, H.P. Frerichs, M. Lehmann, G. Kiss, GasFET for the detection of reducing gases, Sensors and Actuators, B: Chemical 111 (2005) 106–110.
[15] R.E. Presley, C.L. Munsee, C.H. Park, D. Hong, J.F. Wager, D.A. Keszler, Tin oxide transparent thin-film transistors, Journal of Physics D: Applied Physics 37 (2004) 2810–2813.
[16] J. Wollenstein, M. Jagle, H. Bottner, Advanced gas sensing, Kluwer Academic, Boston, 2003, pp. 85–99.
[17] K.K. Purushothaman, M. Dhanasankar, G. Muralidharan, Effect of fluorine content on the morphological, structural, optical and electrical properties of nanostructured SnO_2 films, Surface Review and Letters 14 (2007) 1149–1156.
[18] M. Adnane, H. Cachet, G. Folcher, S. Hamzaoui, Beneficial effects of hydrogen peroxide on growth, structural and electrical properties of sprayed fluorine-doped SnO_2 films, Thin Solid Films 492 (2005) 240–247.
[19] C. Agashe, M.G. Takwale, B.R. Marathe, V.G. Bhide, Structural-properties of SnO_2-F films deposited by spray pyrolysis, Solar Energy Materials 17 (1988) 99–117.
[20] B. Benrabah, A. Bouaza, S. Hamzaoui, A. Dehbi, Sol–gel preparation and characterization of antimony doped tin oxide (ATO) powders and thin films, European Physical Journal-Applied Physics 48 (2009) 30301.
[21] C. Savaniu, A. Arnautu, C. Cobianu, G. Craciun, C. Flueraru, M. Zaharescu, C. Parlog, F. Paszti, A. Van den Berg, Tin dioxide sol–gel derived films doped with platinum and antimony deposited on porous silicon, Thin Solid Films 349 (1999) 29–35.
[22] A.A. Zhukova, M.N. Rumyantseva, A.M. Abakumov, J. Arbiol, L. Calvo, A.M. Gaskov, Influence of antimony doping on structure and conductivity of tin oxide whiskers, Thin Solid Films 518 (2009) 1359–1362.
[23] G.A. Niklasson, D. Ronnow, M.S. Mattsson, L. Kullman, H. Nilsson, A. Roos, Surface roughness of pyrolytic tin dioxide films evaluated by different methods, Thin Solid Films 359 (2000) 203–209.
[24] C. Agashe, S. Mahamuni, Competitive effects of film thickness and growth rate in spray pyrolytically deposited fluorine-doped tin dioxide films, Thin Solid Films 518 (2010) 4868–4873.
[25] M. Ruske, G. Brauer, J. Pistner, U. Pfafflin, J. Szczyrbowski, Properties of SnO_2 films prepared by DC and MF reactive sputtering, Thin Solid Films 351 (1999) 146–150.
[26] T.Y. Yang, X.B. Qin, H.H. Wang, Q.J. Jia, R.S. Yu, B.Y. Wang, J.O. Wang, K. Ibrahim, X.M. Jiang, Q. He, Preparation and application in p-n homojunction diode of p-Type transparent conducting Ga-doped SnO_2 thin films, Thin Solid Films 518 (2010) 5542–5545.
[27] V.M. Jimenez, J.P. Espinos, A. Caballero, L. Contreras, A. Fernandez, A. Justo, A.R. Gonzalez-Elipe, SnO_2 thin films prepared by ion beam induced CVD: preparation and characterization by X-Ray absorption spectroscopy, Thin Solid Films 353 (1999) 113–123.
[28] W. Hamd, Y.C. Wu, A. Boulle, E. Thune, R. Guinebretiere, Microstructural study of SnO_2 thin layers deposited on sapphire by sol–gel dip-coating, Thin Solid Films 518 (2009) 1–5.
[29] E. Kuantama, D.W. Han, Y.M. Sung, J.E. Song, C.H. Han, Structure and thermal properties of transparent conductive nanoporous F: SnO_2 films, Thin Solid Films 517 (2009) 4211–4214.
[30] G. Zhang, B.K. Roy, L.F. Allard, J. Cho, Titanium oxide nanoparticles precipitated from low-temperature aqueous solutions: II. Thin-film formation and microstructure developments, Journal of the American Ceramic Society 93 (2010) 1909–1915.
[31] G. Zhang, B.K. Roy, L.F. Allard, J. Cho, Titanium oxide nanoparticles precipitated from low-temperature aqueous solutions: I. Nucleation, growth, and aggregation, Journal of the American Ceramic Society 91 (2008) 3875–3882.
[32] M. Agarwal, M.R. De Guire, A.H. Heuer, Synthesis of ZrO_2 and Y_2O_3-Doped ZrO_2 thin film using self-assembled monolayers, Journal of the American Ceramic Society 80 (1997) 2967–2981.
[33] B.C. Bunker, P.C. Rieke, B.J. Tarasevich, A.A. Campbell, G.E. Fryxell, G.L. Graff, L. Song, J. Liu, J.W. Virden, G.L. McVay, Ceraminc thin-film formation on functionalized interfaces through biomimetic processing, Science (New York, NY) 264 (1994) 48–55.

[34] S. Yu, J.S. Lee, S. Nozaki, J. Cho, Microstructure evolution of F-doped SiO_2 thin films through liquid phase deposition, Thin Solid Films 520 (2012) 1718–1723.
[35] P.H. Lei, C.D. Yang, Growth of SiO_2 on InP substrate by LPD, Applied Surface Science 256 (2010) 3757–3760.
[36] T.P. Niesen, M.R. De Guire, Review: deposition of ceramic thin films at low temperatures from aquesous solutions, Solid State Ionics 151 (2002) 61–68.
[37] B. Derjaguin, L. Landau, Theory of the stability of strongly charged lyophobic sols and of the adhesion of strongly charged-particles in solutions of electrolytes, Progress in Surface Science 43 (1993) 30–59.
[38] J.W. Verwey, J.G. Overbeek, Theory of the Stability of Lyophobic Colloids, Elsevier, Amsterdam, 1948.
[39] J. Sun, B.V. Velamakanni, W.W. Gerberich, L.F. Francis, Aqueous latex/ceramic nanoparticle dispersions: colloidal stability and coating properties, Journal of Colloid and Interface Science 280 (2004) 387–399.
[40] Y. Saito, Y. Sekiguchi, M. Mizuhata, S. Deki, Continuous deposition system of SnO_2 thin film by the liquid phase deposition (LPD) method, Journal of the Ceramic Society of Japan 115 (2007) 856–860.
[41] Y. Brandrup, E.H. Immergut, in: Polymer Handbook, third ed., Wiley, New York, 1989.
[42] M. Okuya, S. Kaneko, K. Hiroshima, I. Yagi, K. Murakami, Low temperature deposition of SnO_2 thin films as transparent electrodes by spray pyrolysis of tetra-n-butyltin(IV), Journal of the European Ceramic Society 21 (2001) 2099–2102.
[43] C. Agashe, J. Hupkes, G. Schope, M. Berginski, Physical properties of highly oriented spray-deposited fluorine-doped tin dioxide films as transparent conductor, Solar Energy Materials and Solar Cells 93 (2009) 1256–1262.